# Summary of a Numerical Investigation of the Red Chris Operations in Northern British Columbia (NTS 104H/12W) Using the Finite-Discrete Element Method

**T. Shapka-Fels[1], Norman B. Keevil Institute of Mining Engineering, The University of British Columbia, Vancouver, British Columbia, tfels@student.ubc.ca**

Shapka-Fels, T. (2023): Summary of a numerical investigation of the Red Chris operations in northern British Columbia (NTS 104H/12W) using the Finite-Discrete Element Method; *in* Geoscience BC Summary of Activities 2022: Minerals, Geoscience BC, Report 2023-01, p. 71–78.

## Introduction

The transition of open pit to cave mining results in dynamic multidisciplinary challenges during design, operation and closure. The objective of the research summarized in this paper is to investigate the role of numerical analysis applied to the transition problem, and to develop models to understand the geomechanical interaction between open pit and cave mining based on different geological and mine-design variables. Models with special consideration of the planned caving operation at the Red Chris operations (Red Chris) in northern British Columbia (BC) were created using publicly available data.

This paper summarizes the development and highlights results of selected Finite-Discrete Element Method (FDEM) models of the Red Chris operations, as part of research published by Shapka-Fels (2022). The numerical models were developed using the hybrid continuum-discontinuum method, with the software package Elfen (v. 5.2.6) created by Rockfield (2020). FDEM allows for simulation of intact-rock strength parameters; existing fracture networks and geological structures; fracture development due to changes in stress; and kinematic failure mechanisms.

These models represent further study into the numerical modelling challenges in large-scale rock engineering problems, as discussed by Shapka-Fels and Elmo (2022). This study of the Red Chris operations was not sponsored by Newcrest Mining Limited or Imperial Metals Corporation. The study presented herein only utilizes what is publicly available to provide insight into FDEM modelling conceptualization and parameters, and is not intended to replicate conditions at the Red Chris operations or to make technical or financial decisions.

[1]*The lead author is a 2022 Geoscience BC Scholarship recipient.*

*This publication is also available, free of charge, as colour digital files in Adobe Acrobat® PDF format from the Geoscience BC website: http://geosciencebc.com/updates/summary-of-activities/.*

## Red Chris Operations

The Red Chris operations, located in northwestern BC (Figure 1), comprise a currently operating open-pit mine and a planned block-cave underground operation. This copper-gold asset is managed by a joint venture between subsidiaries owned by Newcrest Mining Limited and Imperial Metals Corporation. Combined open-pit and block-cave mine operations were considered at Red Chris prior to commencing mine construction in 2012 (Gillstrom et al., 2012). Updated technical studies forecast the open pit to be completed in 2026, with early cave production planned for the same year (Stewart et al., 2021).

## Model Assumptions and Scenarios

Published information from the 2021 *Red Chris Block Cave Pre-Feasibility Study (PFS)*, as outlined in the latest NI 43-101 technical report (Stewart et al., 2021), was used for the conceptualization of numerical models in this study and is herein referred to as the '2021 PFS'. Certain assumptions for modelling inputs were used to supplement published information. These include base assumptions and variations for model scenarios in terms of material parameters, major structures and preconditioning. The base-case model scenario and three comparative scenarios were selected for discussion in this paper (Table 1).

### Material Parameters

The material parameters used for the Red Chris FDEM models were based on the material parameters for a mine within a similar deposit type.

The material properties for the South Boundary fault zone were approximated, assuming the fault zone is a weak heterogeneous mixture of gouge, breccia and gravel-size clasts. The clayey and granular material is simulated as a weak but brittle material, which will not fail in the FDEM model as it may in reality. This is an important limitation with this method of numerical analysis.

Upscaled material parameters were tested as an attempt to increase the computing speed of the FDEM models. The base FDEM model geometry was re-meshed to a size of 4 m


**Figure 1.** Location of the Red Chris operations in northwestern British Columbia.

within the cave propagation zone, and material properties were upscaled. Different upscaling assumptions were applied based on approaches of modifying the intact-rock parameters (i.e., unconfined compressive strength [UCS]) or the Geological Strength Index (GSI), proposed by Elmo et al. (2010), Elmo and Stead (2017) and Guajardo (2020). This paper presents the results of one scenario tested to highlight the importance of understanding upscaling limitations.

### Structure

Subvertical features are important with regard to caving propagation, thus the evaluation of different structural scenarios was included in the FDEM model investigation. Structural variations were investigated: the first structural scenario contained all the discrete faults within the 2021 PFS, while alternative structural patterns derived from Rees et al. (2015) consider a more complex structural framework that includes primary and secondary structures (splays and relays). The alternative scenarios considered the replacement of moderately dipping faults with two steeply dipping structures that were modified from the interpretation of the Dead Zone (DZ) fault zone presented in Rees et al. (2015).

### Preconditioning

Preconditioning was simulated within the FDEM models as pre-existing horizontal fractures, starting several metres above the undercut level (UCL) and continuing up toward the pit floor. Variations in the height of preconditioning and horizontal extent of the fractures were tested, with one case presented in this paper. The fractures were not continuous through faults and fault zones due to induced damage within the models at intersections and a conceptual idea that the fractures would not propagate through the heterogeneous cataclastic rock material within large fault zones.

## Development of the FDEM Model

The schematic cross-section used in subsidence modelling for the 2021 PFS (location shown in Figure 2) was the basis of the primary FDEM model geometry (Figure 3). The section comprises a UCL that is 715 m below an approximately 300 m deep open pit with a northwest overall slope angle of 40° and a southeast overall slope angle of 37°. The caving UCL is 360 m in width, with an initial excavation height of 1 m. The entirety of the model measures 2640 m by 1100 m,

**Table 1.** Selected 2-D conceptual Finite-Discrete Element Method (FDEM) modelling scenarios for the Red Chris operations.

| Model | Description |
|---|---|
| 2.1 | Base case scenario. |
| 2.6 | Upscaling materials using 88% unconfined compressive strength. Scaled caving area mesh size from 2 m to 4 m. |
| 2.7 | Modified structural pattern with steeply dipping faults and shallow northwest-dipping faults. |
| 2.11 | Modified structural pattern with steeply dipping faults and shallow northwest-dipping faults. Hydrofractures span the footprint laterally with partial extension of 40 m to the northwest. The hydrofractures continue at 4 m spacing vertically to midway between the undercut level and pit floor. |

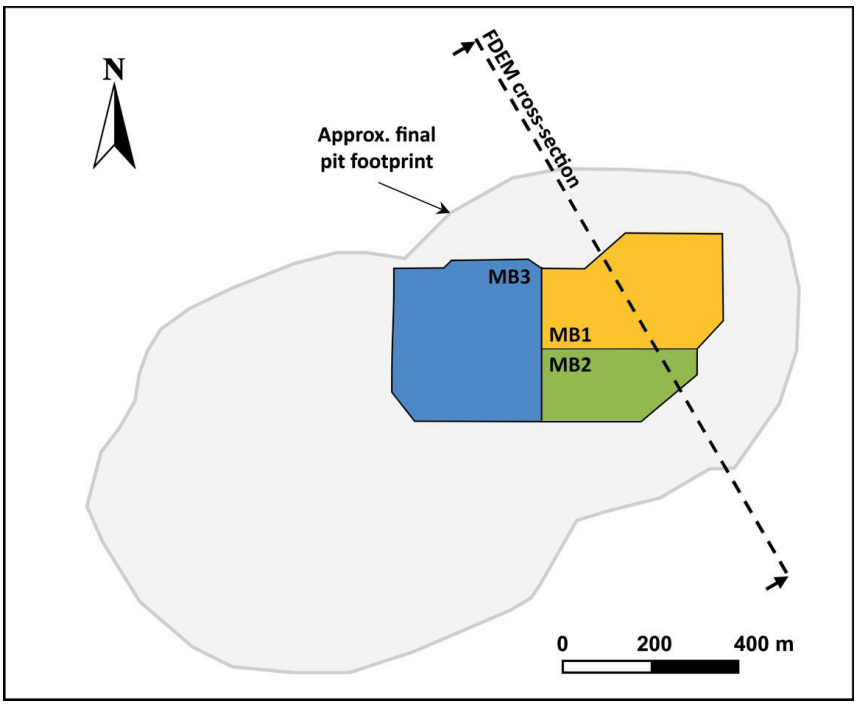


**Figure 2.** Location of cross-section used in FDEM modelling, relative to the Red Chris final pit footprint and macroblocks.

subdivided into elastic and elastoplastic regions with fracturing. The nonfracturing elastic region is required to minimize boundary effects and is modelled with a lower mesh resolution. The open pit is modelled elastically and excavated in four 70–80 m stages. The structures considered in all models include the South Boundary fault zone and the East Zone (EZ) fault. Alternate structural scenarios replace the Hanging Wall (HW1 and HW2) faults in the primary FDEM model with reinterpreted faults in the DZ fault zone and include shallow dipping faults.

Mesh resolution varies at 1 m within the UCL and 2 m above the undercut up to the pit bottom, and increases to 40 m near the model boundaries. The upscaled scenarios have a mesh size of 4 m within the cave propagation zone

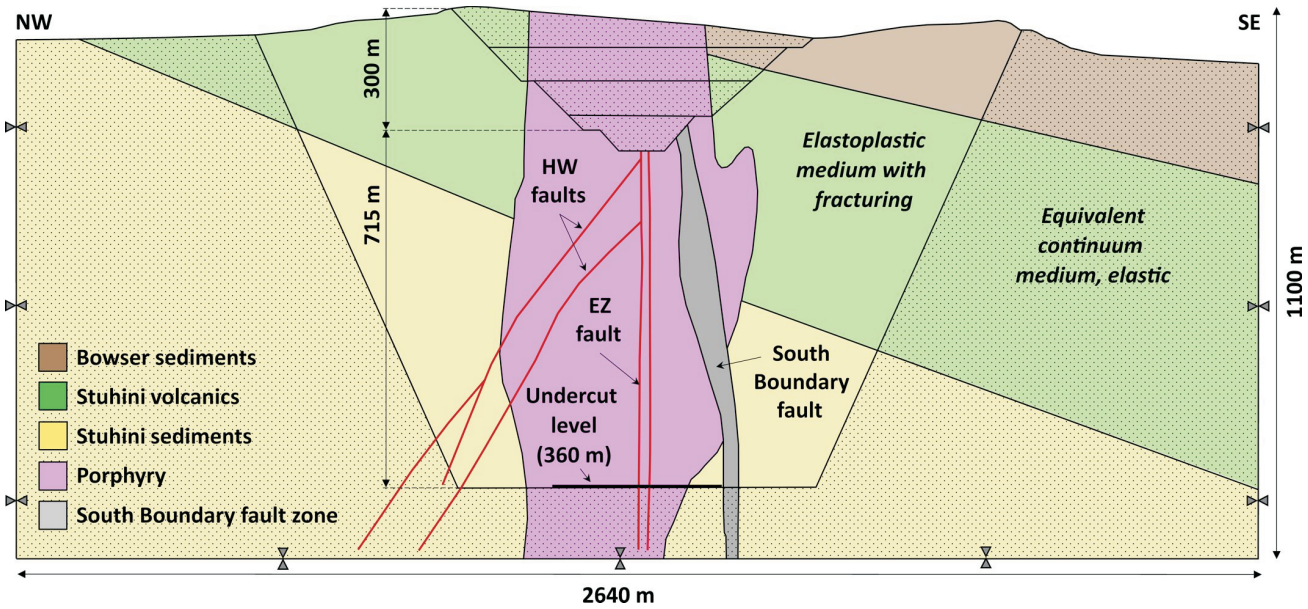


**Figure 3.** Schematic diagram of base FDEM geometry and boundary conditions for Red Chris Models 2.1 and 2.6. Dotted regions indicate elastic material, while solid regions are modelled as elastoplastic regions with fracturing. Abbreviations: EZ, East Zone (Fault); HW, Hanging Wall (Fault); NW, northwest; SE, southeast.

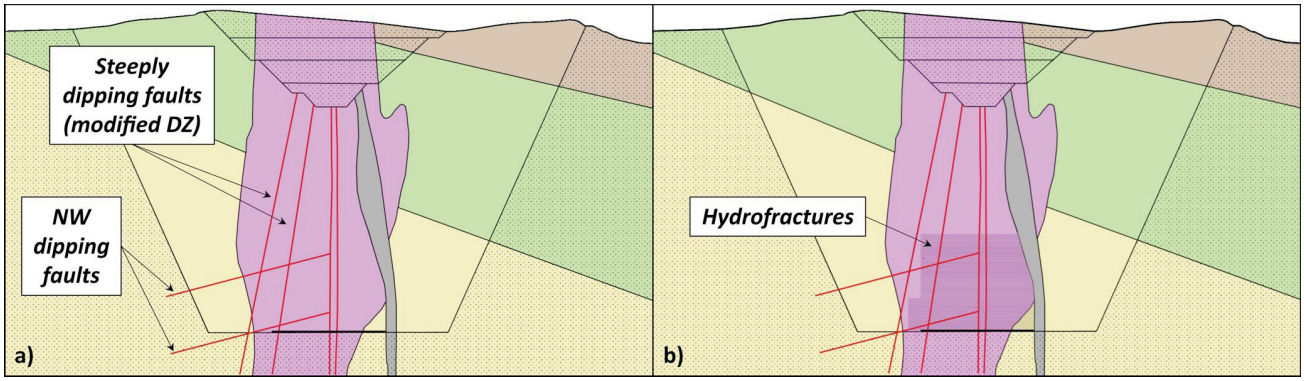


**Figure 4.** Schematic diagrams illustrating variations from the base FDEM geometries for **a)** Red Chris Model 2.7, with an alternate structural setting, and **b)** Red Chris Model 2.11, with an alternate structural setting and preconditioning. Abbreviations: DZ, Dead Zone (Fault), NW, Northwest.

(changed from 2 m). Model geometry variations described in Table 1 are illustrated in Figure 4.

## Results from the FDEM Model

Conceptual Red Chris–based FDEM models were created to investigate the effects of structural variability, material upscaling and preconditioning. Due to the variation in model timing, comparable models were selected at a specific 2-D production value. Model results are presented after a 2-D production of 21 300 $m^2 \pm 5\%$ (Figures 5–8). Height of draw (HOD) is reported as the maximum Y displacement, and model time is reported as time past the first deletion. Crater depth corresponds to the Y displacement at the pit floor.

In the majority of the models, slope failure and mobilization occurred due to caving-induced unloading; however, the magnitude of movement varied greatly between models.

The following subsections contain observations for each model based on the differences relative to Model 2.1 (Figure 5) at the same level of 2-D production, unless otherwise specified. Differences in total displacement (XY), HOD and model run times are reported in the corresponding summary figures. The resulting figures showcase the area of in-

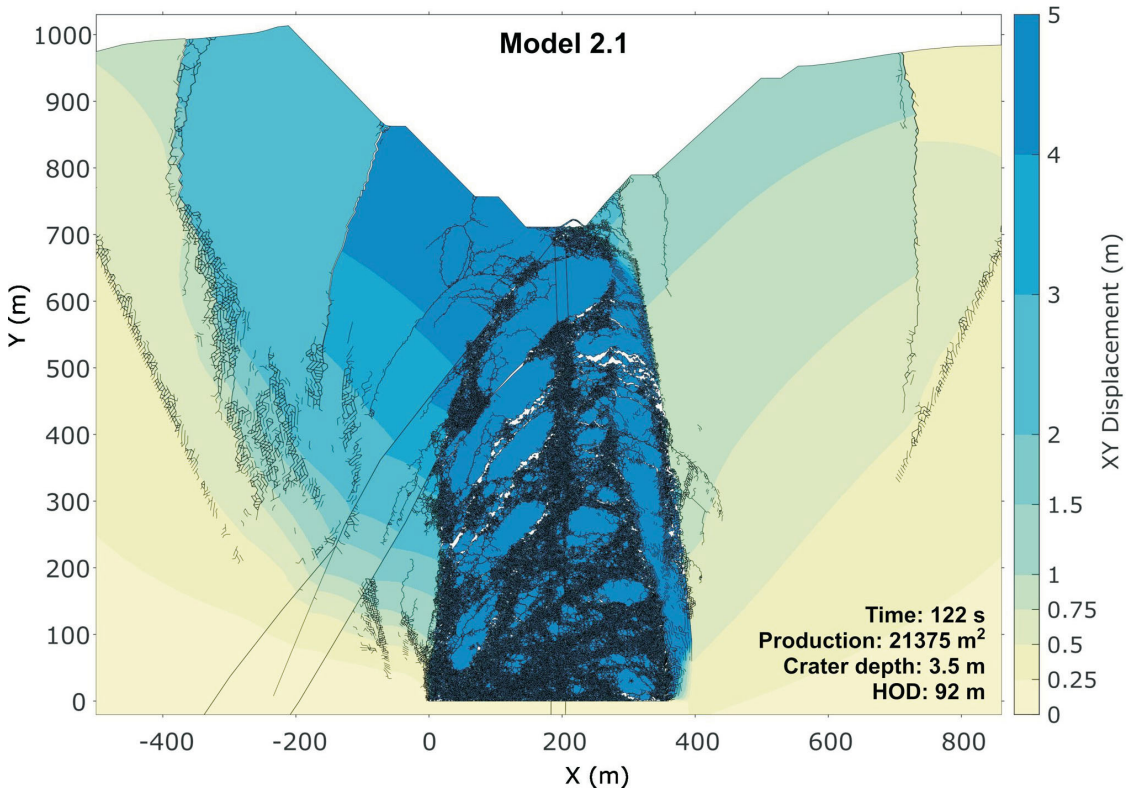


**Figure 5.** FDEM results for Red Chris Model 2.1, with XY displacement (m) contours. Abbreviations: HOD, height of draw (maximum vertical displacement at undercut level).

terest (i.e., fracturing area) within the overall model boundaries.

Model 2.1 (Figure 5) exhibits early fracturing (prior to cave initiation) near the pit floor resulting from the intersecting faults and rebound post excavation. Displacement of the lower southeast inter-ramp slope can be attributed to the weak material of the South Boundary fault zone. Maximum vertical displacement was located on the northwest side of the UCL, as expected with the draw sequence and timing.

The cave propagated at a greater rate southeast of the EZ faults, likely due to the stress conditions resulting in a greater stress ratio between the subvertical faults and the South Boundary fault zone. The HW faults provided some level of resistance to cave propagation; however, continued production and displacement of the northwest pit slope rendered these structures obsolete. The southeast boundary of the South Boundary fault zone limited the extent of the caved material, until production was such that major fracturing extended to the southeastern lithological contact of the Porphyry and the Stuhini volcanics. Due to the orientation of the South Boundary fault zone, continued production resulted in enough vertical displacement that an overhang was created. Without support of caved material below, the overhanging material fell and much of the southeast pit wall was included in the main cave body.

## Upscaling Method

Model 2.6 (Figure 6) was selected to highlight the effects of upscaling. Model 2.6 was the only model in this study resulting in a stalled cave propagation and a large air gap. This model is significant because it exemplifies how material-input parameters are not independent from the mesh size. Without reducing the material strength enough to account for the mesh size increase, the model results in a very different outcome.

There was minimal interaction between the cave and the open pit. The cave started stalling at a stage of propagation similar to Model No. 2.1 at 97 seconds (48 seconds past first deletion), and the air gap continued to grow as production continued. Despite the stress concentration, the fracturing did not continue because of the relative strength of the material.

## Structural Pattern

The Red Chris Model 2.7 (Figure 7) was selected to highlight the effects of different structural scenarios on cave propagation, particularly discrete subvertical faults. The main fracturing area in Model 2.7 was controlled by the modified DZ faults, resulting in narrowing as the cave propagated toward the pit bottom. The fracturing is more limited by the southeast DZ fault because fracturing did not

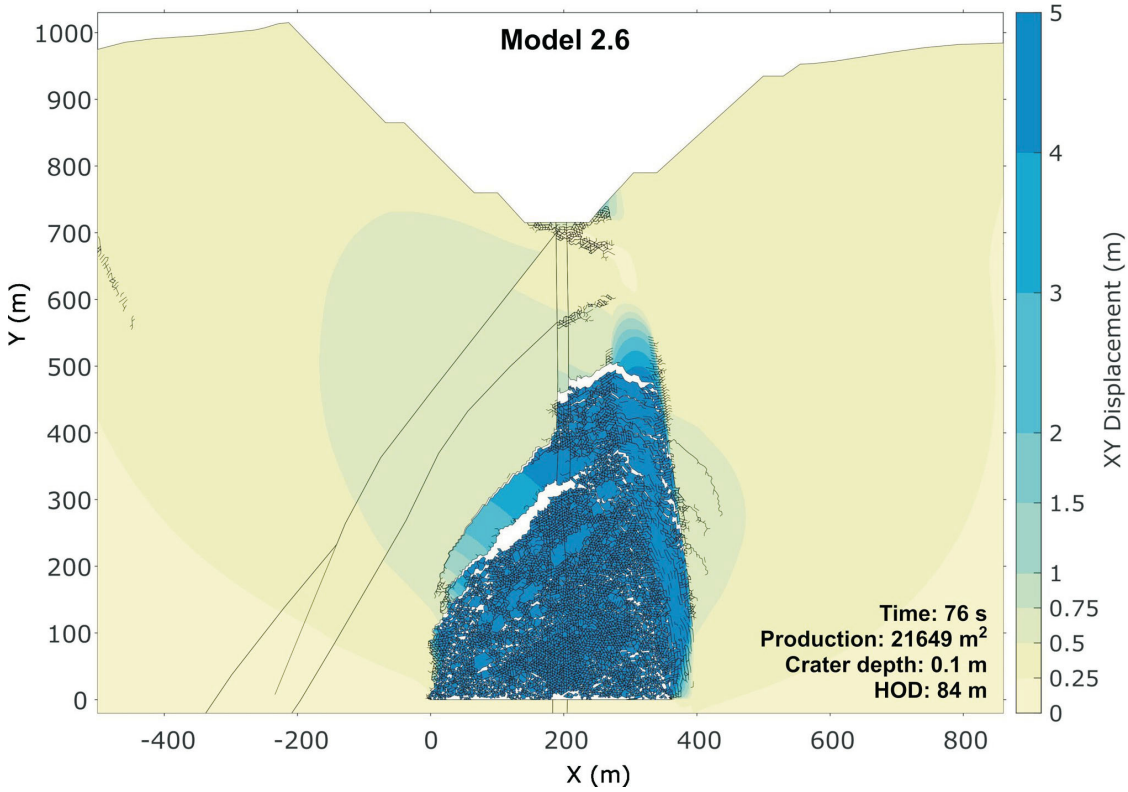


**Figure 6.** FDEM results for Red Chris Model 2.6, with XY displacement (m) contours. Abbreviations: HOD, height of draw (maximum vertical displacement at undercut level).

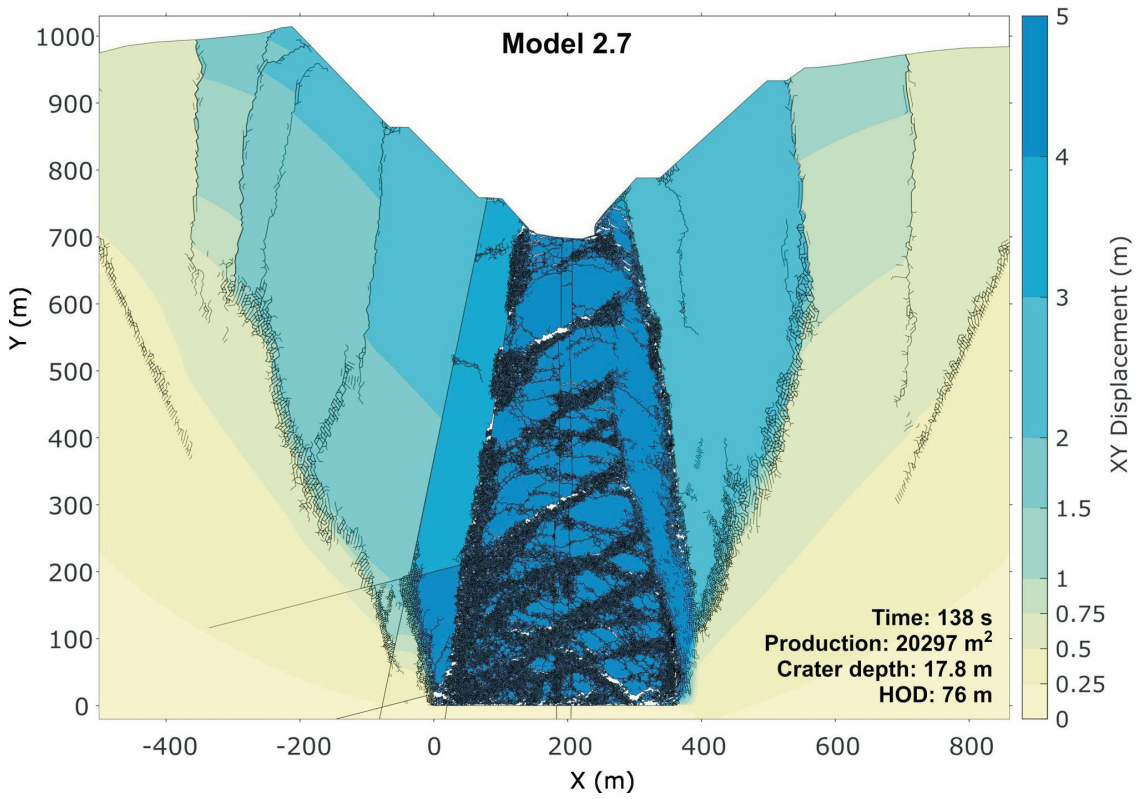


**Figure 7.** FDEM results for Red Chris Model 2.7, with XY displacement (m) contours. Abbreviations: HOD, height of draw (maximum vertical displacement at undercut level).

continue through the discrete feature, except where the shallow dipping faults intersected the DZ faults above the UCL. Cave propagation was overall more symmetrical with this structural scenario, as the high stress ratio (and horizontal stresses) were distributed between the South Boundary fault zone and the DZ faults. The larger subsidence zone included both pit walls up to the top of the pit, also with more symmetrical displacement.

Higher initial vertical displacement (defined by 1 m of movement) occurred on the southeast side of the UCL; however, subsequent vertical displacement was higher on the northwest side, as per the production sequencing. Increased fracturing occurred in a pattern of bands that dip at shallow to moderate angles toward the northwest, with lesser conjugate bands dipping to the southeast.

### Preconditioning

Model 2.11 was selected to highlight the effects of preconditioning (Figure 8), using pre-existing horizontal discontinuities. This model contained the same structural pattern as Model 2.7. In comparison to Model 2.7, the addition of hydrofractures resulted in a more symmetrical and centralized cave propagation with less deformation of the pit slopes above the lower ramps (Figure 7).

Fragmentation resulting from the introduction of hydrofractures increased relative to the spacing heights between hydrofractures. Above the hydrofractures, increased fracturing occurred along the southeast DZ fault, but significant deformation occurred between the two DZ faults as well. This could be attributed to the hydrofractures causing fracturing damage and connection between the two faults, in contrast to Model 2.7 (at earlier stages).

The contrast between the continuum material and the hydrofractured areas provided a boundary for caving-induced fracturing to follow, limiting the extent of fracturing beyond the hydrofractured areas. However, extending the hydrofractures outside the footprint area did not cause increased fragmentation, fracturing or recovery of material in that area. Increasing the height of hydrofractures in this extended area may have caused better connection between the shallow dipping faults (as seen in Model 2.7, Figure 8), resulting in a different magnitude of deformation on the northwest side.

## Learnings

An FDEM investigation was completed for a case study on the Red Chris operations and planned block-cave mine, albeit with many assumptions applied due to the lack of publicly available geotechnical information. The models presented in this paper are considered investigative forward-analysis models, created to further understand cause-and-effect of upscaling, structural geology and preconditioning

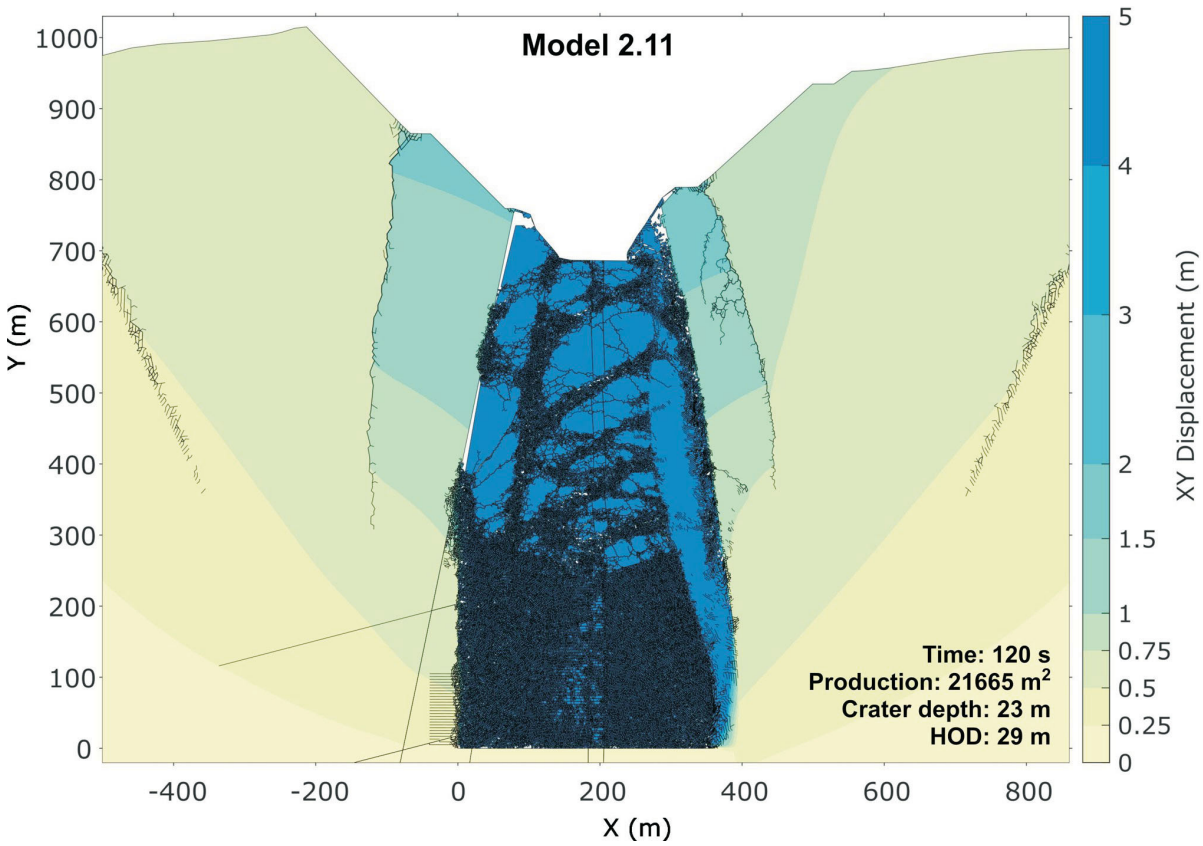


**Figure 8.** FDEM results for Red Chris Model 2.11, with XY displacement (m) contours. Abbreviations: HOD, height of draw (maximum vertical displacement at undercut level).

to predict cave-propagation processes. Results were presented based on each individual model; however, the key learnings from these models extend beyond the individual scenarios. While these models are 2-D, the same limitations discussed would apply to 3-D models, although 3-D models with the same fracturing capabilities would have significantly greater run times, thus rendering them impractical for investigative risk-based analysis. Key learnings from the Red Chris FDEM models are grouped under the following five subsections.

## Common Modelling Artifacts

Large tension cracks occur in most models, resulting in significant deformation of the pit slopes. In models without a discrete fracture network (DFN), tension cracks may form due to the buildup of strain within the rock-mass continuum. Generally, cracks preferentially develop along material boundaries, whether lithological or defined fracturing limits. Also related to continuum-modelling artifacts is the fracturing damage at fault intersections due to the concentration of movement toward and along those discrete fault planes when the rest of the rock mass is modelled as a continuum (i.e., no DFN).

After large excavations, such as the excavation of the pit, the rebound of unexcavated material may cause fracturing, particularly in the pit floor. Increasing relaxation times and equilibrium stages may reduce fracturing, but this possibility was not tested as part of this study. Beams of unbroken elements form near the pit floor after deformation of the pit slopes cause squeezing. The cut-off strength between elements has not been reached, and these beams can be considered a relic of continuum rock masses. These beams also commonly occur when modelling hydrofractures as straight and horizontal features.

## Induced-Stress Field

The stress ratio increases (i.e., horizontal stresses greater) below the pit floor as the pit is excavated. Early stages of caving result in horizontal stresses concentrating between subvertical faults within the cave-propagation zone, as the horizontal stresses cannot be transmitted across the discrete features. In models that contain hydrofractures, high stress ratios occur in an ellipsoidal shape centred above the caved material, as well as between subvertical faults. This is likely the cause of the increased speed of vertical movement of the cave back, and is due to the limited translation of vertical stresses across the horizontal fractures.

### Fault-Material Parameters

If a particular fault zone has a high composition of granular material, it would be expected to unravel into the caved material and increase fines reporting to the production level. However, the mesh size is a limiting factor to model this concept, as it would have to be significantly finer to capture the same process.

### Upscaling

Properties of rock-mass material are not unique to the geotechnical domain, but rather to both the material and the scale of discretization. Often, materials are modelled with a change in discretization scale such that mesh sizes are smaller in regions where fracturing is more expected. This raises an important consideration: with material parameters dependent on mesh size, when does a modeller start upscaling?

### Preconditioning

Preconditioning changes the stress regime significantly, with early vertical propagation of the cave reaching the pit floor at lower production levels. The hydrofractures also add contrast boundaries, resulting in certain control over the location of cave propagation. However, adding hydrofractures above the UCL but outside the footprint area may not increase recovery.

Modelling hydrofractures comes with another suite of challenges, regardless of modelling method. Decisions include whether hydrofractures remain continuous through faults and the timeline of their creation (i.e., cannot be inserted at different stages). There is also limited understanding of how to implement realistic development of fractures during the preconditioning process due to incremental changes in principal stress orientation.

## Conclusions

This paper highlights a portion of a completed thesis with research that has contributed to the field of numerical analysis in rock engineering by highlighting important aspects of numerical analysis applied to the study of large-scale problems, particularly pit-to-cave transition.

In FDEM models, a large focus of the process and conceptualization should be on rock-mass discontinuities—whether they be major structural features (i.e., faults and fault zones), discrete fracture networks and rock-mass fabrics, or induced hydrofractures for preconditioning for caving. These features impact primary failure mechanisms observed in the open pit–to–cave FDEM models, as well as magnitude of deformation, due to their effects on stress continuity.

## Acknowledgments

The author would like to acknowledge D. Elmo (University of British Columbia) and L. Zorzi (Golder/WSP) for providing comments and assistance, and the financial contributions of Geoscience BC through their graduate scholarship program.

## References

Elmo, D., Rogers, S., Beddoes, R. and Catalan, A. (2010): An integrated finite/discrete element method – discrete fracture network synthetic rock mass approach for the modelling of surface subsidence associated with panel cave mining at the Cadia East underground project; *in* Caving 2010: Proceedings of the Second International Symposium on Block and Sublevel Caving, Y. Potvin (ed.), Australian Centre for Geomechanics, April 20–22, 2010, Perth, Australia, p. 167–179, URL <https://doi.org/10.36487/ACG_rep/1002_9_Elmo>.

Elmo, D. and Stead, D. (2017): Applications of fracture mechanics to rock slopes; Chapter 23 *in* Rock Mechanics and Engineering, Volume 3: Analysis, Modeling & Design, X.-T. Feng (ed.), CRC Press, p. 705–735, URL <https://doi.org/10.1201/b20402>.

Gillstrom, G., Anand, R., Robertson, S. and Sterling, P. (2012): 2012 technical report on the Red Chris copper-gold project; National Instrument 43-101 report prepared for Imperial Metals Corporation, 334 p., URL <https://imperialmetals.com/assets/docs/2012-Red-Chris-43-101-Report.pdf> [March 2021].

Guajardo, C.A. (2020): Numerical investigation on strength upscaling and its application to a back analysis of an open pit slope failure; M.A.Sc. thesis, The University of British Columbia, 136 p., URL <https://open.library.ubc.ca/soa/cIRcle/collections/ubctheses/24/items/1.0388530> [November 2022].

Rees, C., Riedell, K.B., Proffett, J.M., Macpherson, J. and Robertson, S. (2015): The Red Chris porphyry copper-gold deposit, northern British Columbia, Canada: igneous phases, alteration, and controls of mineralization; Economic Geology, v. 110, no. 4, p. 857–888, URL <https://doi.org/10.2113/econgeo.110.4.857>.

Rockfield (2020): Elfen version 5.2.6; Rockfield Software Ltd., URL <https://www.rockfieldglobal.com> [November 2022].

Shapka-Fels, T. (2022): Numerical analysis of the geomechanical interaction between open pit and cave mining using the hybrid finite-discrete element method; M.A.Sc. thesis, The University of British Columbia, 138 p., URL <https://open.library.ubc.ca/soa/cIRcle/collections/ubctheses/24/items/1.0418437> [November 2022].

Shapka-Fels, T. and Elmo, D. (2022): Numerical modelling challenges in rock engineering with special consideration of open pit to underground mine interaction; Geosciences, v. 12, no. 5, p. 199, URL <https://doi.org/10.3390/geosciences12050199>.

Stewart, R., Swanson, B., Sykes, M., Reemeyer, L., Wang, B. and Stephenson, P. (2021): Red Chris Operations, British Columbia, Canada, NI 43-101 Technical Report; National Instrument 43-101 report prepared for Newcrest Mining Ltd. and Imperial Metals Corporation, 285 p., URL <https://www.newcrest.com/sites/default/files/2021-11/211130_Newcrest%20Technical%20Report%20on%20Red%20Chris%20Operations%20as%20of%2030%20June%202021.pdf> [March 2022].